



C: Surfaces, Interfaces, Porous Materials, and Catalysis

Structure and Dynamics of an Ionic Liquid Mixture Film Confined by Mica

Waruni V Karunaratne, and Claudio Javier Margulis

J. Phys. Chem. C, Just Accepted Manuscript • DOI: 10.1021/acs.jpcc.9b05510 • Publication Date (Web): 05 Aug 2019

Downloaded from pubs.acs.org on August 9, 2019

Just Accepted

"Just Accepted" manuscripts have been peer-reviewed and accepted for publication. They are posted online prior to technical editing, formatting for publication and author proofing. The American Chemical Society provides "Just Accepted" as a service to the research community to expedite the dissemination of scientific material as soon as possible after acceptance. "Just Accepted" manuscripts appear in full in PDF format accompanied by an HTML abstract. "Just Accepted" manuscripts have been fully peer reviewed, but should not be considered the official version of record. They are citable by the Digital Object Identifier (DOI®). "Just Accepted" is an optional service offered to authors. Therefore, the "Just Accepted" Web site may not include all articles that will be published in the journal. After a manuscript is technically edited and formatted, it will be removed from the "Just Accepted" Web site and published as an ASAP article. Note that technical editing may introduce minor changes to the manuscript text and/or graphics which could affect content, and all legal disclaimers and ethical guidelines that apply to the journal pertain. ACS cannot be held responsible for errors or consequences arising from the use of information contained in these "Just Accepted" manuscripts.

Structure and Dynamics of an Ionic Liquid Mixture Film Confined by Mica

Waruni V. Karunaratne and Claudio J. Margulis*

Department of Chemistry, University of Iowa, Iowa City, Iowa 52242, United States

E-mail: claudio-margulis@uiowa.edu

Abstract

In a recent article (J. Phys. Chem. C 2019, 123, 4914–4925) we studied using molecular dynamics simulations the structure of an ionic liquid (IL) mixture comprised of 1-methyl-3-octylimidazolium octylsulfate and 1-ethyl-3-methylimidazolium ethylsulfate confined by vacuum interfaces. At these interfaces, the mixture formed an apolar blocking layer concealing the smaller and more polar ions to the interior of the liquid phase. In the current work, and for the same IL mixture, we study the case of confinement between (001) mica surfaces, where the solid provides a flat and polar ionic interface. Our focus is twofold; first, we want to understand the structural and dynamical behavior of the IL mixture at the boundary where the confining interface is highly polar and second we want to establish how far away from the interface liquid behavior is recovered. This last point is particularly important in light of puzzling recent experimental results regarding the behavior of ILs and solutes dissolved in them under confinement where large distances appear to be necessary to recover true bulk behavior. We find that the IL mixture is highly structured at the adlayer, but within 5 nm bulk-like structural features are recovered. Dynamical properties at the center of our thin film also appear converged to bulk behavior, but further studies are required to fully address the issue of dynamics within confined IL films.

Introduction

Ionic Liquids (ILs) have unique chemical and physical properties which make them excellent candidates for various applications in chemical synthesis, catalysis, lubrication and electrochemistry among other areas and they can be designed with specificity for particular problems. 1-5 The design for particular purposes needs not be restricted to the combination of a single cation with a single anion and many studies have gone beyond this by considering mixtures with conventional solvents or multiple ions. Significant research has recently been devoted to binary and ternary mixtures of ILs. 6-16 Because this is relevant to applications, when dealing with multiple salt components, we are not only interested in their bulk behavior but also in their preferential arrangement at interfaces.

A substantial number of experimental and theoretical studies have already been carried out on ILs at interfaces, and highlighted in recent review articles. ^{2,3} In these studies, researchers have discussed patterns of interface—induced order. Recently, using atomic force microscopy, Atkin and coworkers found that the structure of ILs at the mica interface was sensitive to the ion size, solvophobicity and hydrogen bonding ability; ^{2,17} using neutron reflection combined with the surface force balance technique, Norman and coworkers revealed the nature of density oscillations of an IL between mica sheets. ¹⁸ Several simulation studies also addressed the structure of ILs at neutral and charged mica interfaces. ^{19–25} For the most part, studies appear to agree that beyond a few nanometers interfacial structural effects decay to bulk behavior.

Somewhat puzzling, is recent work that hints at the possibility of surface—induced effects that do not dissipate at short distance (a few nanometers) from the interface, especially when confinement is coupled to external forces. ^{26–28} In particular, reports exist that suggest the dynamics of ILs under confinement (inside membrane pores or in films ^{29–31}) and that of solutes dissolved in them, could be notably slow when compared to bulk behavior under the same conditions.

The gap in our current understanding about IL mixtures at interfaces as compared to the bulk has been prominently highlighted in the literature. ¹¹ In a recent study, we explored the organization of a 50% mixture of 1-methyl-3-octylimidazolium octylsulfate (C[8]-mim⁺/C[8]- OSO_3^-) and 1-ethyl-3-methylimidazolium ethylsulfate (C[2]-mim⁺/C[2]- OSO_3^-) confined by vacuum. ³² We found that if the film was thinner than the decay length for spatial correlations away from the interface (\sim 6 nm), ions were highly organized. However, in thicker films of about 24 nm, a bulk-like liquid region with a flat atomic density profile could be clearly observed if careful ³² temporal averaging was carried out. As pointed out in that study, for ionic liquids that have mesoscale structure in the bulk, a well converged atomic density profile

away from the interface requires very long simulations (hundreds of nanoseconds). This is because of the need to average out the random equilibrium configurations of the nanoscale domains. This must be done in order to distinguish the oscillations in the density profile caused by the interface from the same-type polar-apolar oscillations naturally occurring in the bulk. The difference between these two is that oscillations caused by flat boundaries are directional, whereas polar-apolar domain alternations in the bulk are not; the key issue is that in a simulation, these are indistinguishable if averaging is insufficient. Many prior studies have not properly addressed this and hence were unable to unequivocally distinguish the two types of density fluctuations.

Besides studying the structure and dynamical behavior of our mixture of ILs at a highly polar interface in comparison with the highly apolar vacuum interface described in reference 32, we would also like to start addressing the somewhat controversial question of whether the "bulk–like" interior of an IL or mixture of ILs in nanoconfined environments is structurally and dynamically distinguishable from "real" bulk. In particular, we focus on whether beyond the interfacial structural persistence length-scale, the liquid exhibits structural or dynamical characteristics that deviate from the perfectly unperturbed bulk. Our simulated film composed of 50% C[8]-mim $^+$ /C[8]-OSO $_3^-$ and C[2]-mim $^+$ /C[2]-OSO $_3^-$ confined between (001) mica surfaces (see Figs 1 and 2), is relevant in the context of surface force measurements and atomic force microscopy studies reported by the Espinosa-Marzal and Atkin groups. 17,26,33,34

2 Simulation Details

Muscovite mica, KAl₂Si₃AlO₁₀(OH)₂, is a monoclinic clay mineral that can easily produce a well-defined, atomically flat (001) surface.³⁵ A single layer of mica has a tetrahedraloctahedral-tetrahedral (TOT) structure in which an ocatahedral Al sheet is enclosed between two tetrahedral Si sheets. Some of the Si⁴⁺ are substituted by Al³⁺ giving rise to a net negative charge which is neutralized by interlayer K⁺ ions. There is a long-standing

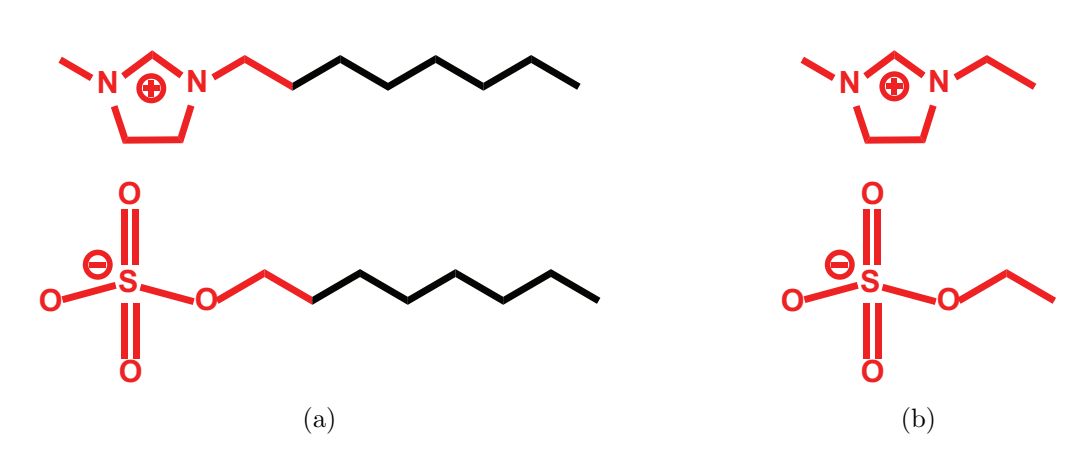


Figure 1: Molecular structures of (a) C[8]-mim⁺/C[8]-OSO $_3^-$ and (b) C[2]-mim⁺/C[2]-OSO $_3^-$. Red and black denote the definition of polar and apolar ionic subcomponents used throughout the article.

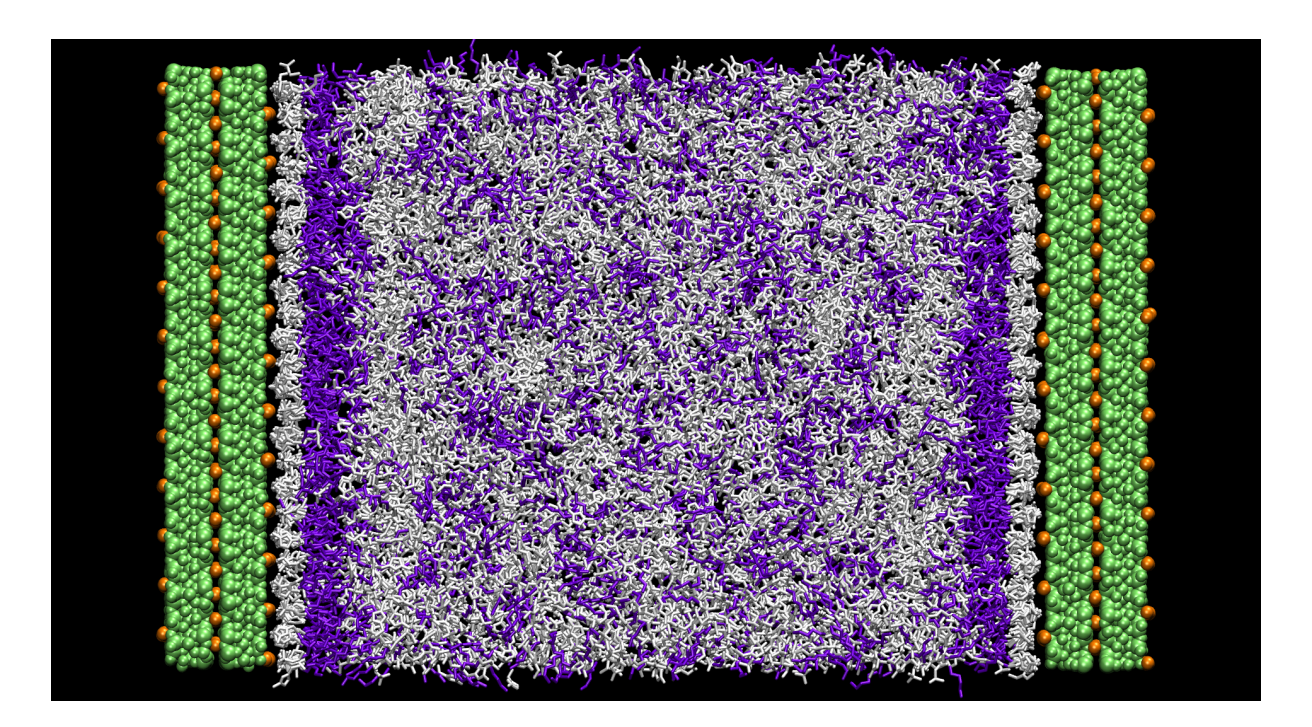


Figure 2: Final snapshot of our production run at 425 K. Mica is represented as green spheres, K⁺ ions as orange spheres, the polar component of the liquid mixture as defined in Fig. 1 is represented with white wires whereas the apolar components with purple wires. The IL mixture adlayer is highly structured and polar and beyond it an apolar bilayer can be observed followed on the liquid side by a second more disordered polar layer.

controversy in the literature regarding the fate of K^+ ions at the cleaved mica surface and hence its overall charge. $^{36-40}$ This article does not attempt to resolve this controversy; instead our perspective is that ideally in freshly cleaved mica, K^+ ions are uniformly distributed at Si_4Al_2 ring sites 41 on the surface rendering the solid neutral. $^{42-44}$ As time evolves, K^+ ions are free to diffuse or exchange with cations in the IL if that is energetically favorable. We will see in subsequent sections that this phenomenon is not observed on a time scale of a couple of hundred nanoseconds. This is consistent with the hypothesis put forth in the recent literature $^{38-40}$ suggesting that water or other impurities may be important in the diffusion of K^+ ions away from the interface. In the present study, a single crystallographic unit cell of mica 45 was repeated 21 times along the a vector and 12 times along the b vector to obtain a (001) surface that mimics the freshly cleaved conditions of mica. As in prior studies, $^{19,20,35,46-48}$ the 95.8^o monoclinic angle (β) was approximated to 90^o during simulation.

The CLAYFF⁴⁹ force field was used for mica together with the Canongia–Lopes and Pádua^{50,51} and Optimized Potentials for Liquid Simulations All–Atoms (OPLS–AA) force fields.^{52–54} As in our recently published work,³² the charges on the IL were scaled at 78% of their nominal value. This is important to match dynamical properties while still preserving the correct bulk structure function.³² A caveat in these simulations is that the original Canongia–Lopes and Pádua^{50,51} force field uses geometric combination rules for Lennard–Jones interactions whereas the CLAYFF⁴⁹ force field is best used with Lorentz-Berthelot mixing rules.⁵⁵ Our bulk IL simulations follow the original Canongia–Lopes and Pádua prescription, but simulations including mica use Lorentz-Berthelot mixing rules for all atoms. The change introduced, results in negligible (less than 2%) adjustments to the sigma value for cross terms in the IL but are needed to make the two force fields compatible for simulation.

All Molecular Dynamics (MD) simulations were performed using the Gromacs package^{56–58} and used the Nose–Hoover algorithm^{59,60} to control the temperature. The leap–frog algorithm⁶¹ along with a time step of 1 fs was used to integrate all equations of motion.

Our IL mixture consists of 1500 ions of each type (6000 ions total) and equilibration

simulations start from the final (thoroughly equilibrated) bulk liquid configuration obtained from an NPT production run carried out at 650 K for 60 ns in our previous study. ³² Before combining solid slabs with the bulk IL mixture to generate a film geometry, the mica surfaces were energy minimized and relaxed in an NVT simulation for 3 ns at 650 K. Still at 650 K, the combined mica–IL mixture system was first subjected to a semi–isotropic NPT simulation using the Parrinello–Rahman barostat ⁶² to allow the total volume of the system to properly converge by only varying the box length in the z direction. The final equilibrated box dimensions at this point were 10.9 nm x 10.8 nm x 20.6 nm and the simulation was further extended in the NVT ensemble for another 0.25 ns. The Particle Mesh Ewald (PME) method ^{63,64} (EW3D in Gromacs) with an interpolation order of 6 and Fourier grid spacing of 0.8 nm was used while fixing the the short–range Coulomb and Lennard–Jones cutoffs to 1.5 nm.

At this point, the system was placed at the center of a 10.9 nm x 10.8 nm x 82.4 nm rectangular parallelepiped with sufficient empty space to properly apply the EW3DC ^{65,66} PME technique by Yeh and Berkowitz which approximates the 2D Ewald summation appropriate for slab simulations. Subsequent simulation steps were carried out in the *NVT* ensemble. The simulation slab was allowed to relax for 8 ns during which an annealing protocol gradually lowered the temperature from 650 K to 425 K. At the end of this step, we carried out a 200 ns production simulation at 425 K; Figure 2 is a snapshot of its last configuration frame. This run was used to analyze the behavior of our IL mixture confined by mica.

In a separate simulation, the last snapshot of a 60 ns NPT production run performed for the bulk IL mixture at 425 K from our previous study³² was extended in the NVT ensemble for 200 ns at the same temperature. This trajectory was used to determine the structural and dynamical properties of the bulk liquid in the absence of interfaces.

3 Results and Discussion

At the freshly cleaved mica interface, our IL mixture is highly organized. We can begin to see this from the simulation snapshot in Fig. 3 displaying rows of surface K^+ ions in contact with the IL mixture. Each surface K^+ ion appears capped either by C[8]-OSO $_3^-$ or

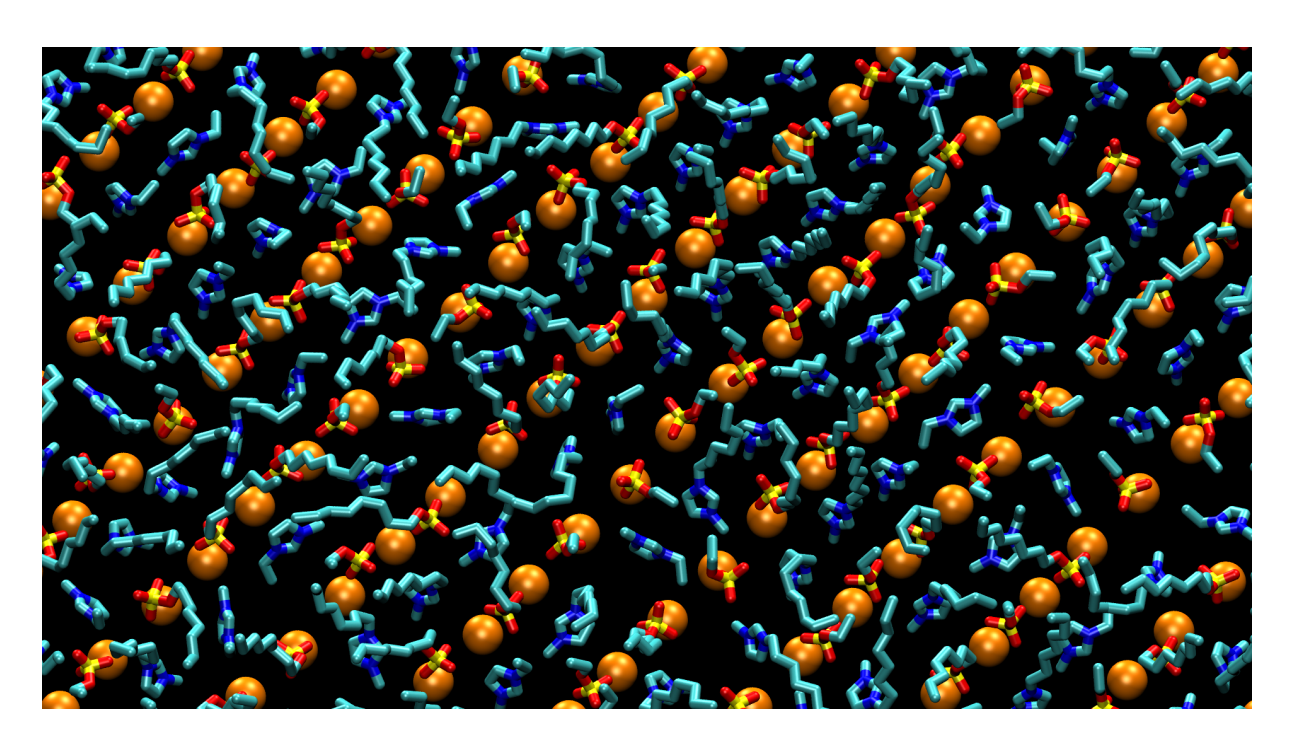


Figure 3: Visualization of surface K^+ ions in contact with the IL mixture. Rows of K^+ ions (orange spheres) are capped from above by sulfate groups of long and short IL anions. Short– and long–tailed imidazolium ions at the interface lay between rows of K^+ ions.

by C[2]-OSO $_3^-$, and the intervening space between rows of K^+ ions is occupied either by C[2]-mim $^+$ or C[8]-mim $^+$. To better understand how this order dissipates into the liquid phase, in subsequent subsections we discuss computed atomic density profiles away from the interface as catalogued by charge, the polar or apolar nature of the components and the type of ions in our IL mixture. We also, discuss the orientation of ions as a function of distance to the interface as well as tangential structural and dynamical correlation functions that help us better understand the transition between the interface into the "liquid–like" region.

3.1 Density Profiles

The final 180 ns of our production trajectory were used to generate all the density profiles along the z direction of our simulation box; this is the direction normal to the interface. Figure 4 (left) shows density variation based on the polarity of ionic subcomponents as defined in Fig. 1. The polar liquid subcomponents comprise the immediate adlayer of the mica substrate followed by an apolar density layer. This pattern of oscillations continues into the liquid phase; if we consider the whole film, we can observe three polar layers and two apolar layers that alternate away from each mica boundary. Beyond about 5 nm, the density profile is flat, indicating the full decay of surface-induced structural oscillations.

Separation of the polar components into the density of each charge type, reveals the existence of two oppositely charged sublayers in direct contact with the interface but at slightly different z values. The cationic layer is closest to the surface; this can be easily understood from Fig. 3 where cationic rings lay in grooves between rows of K^+ ions whereas sulfate anions cap K^+ ions from the liquid side.

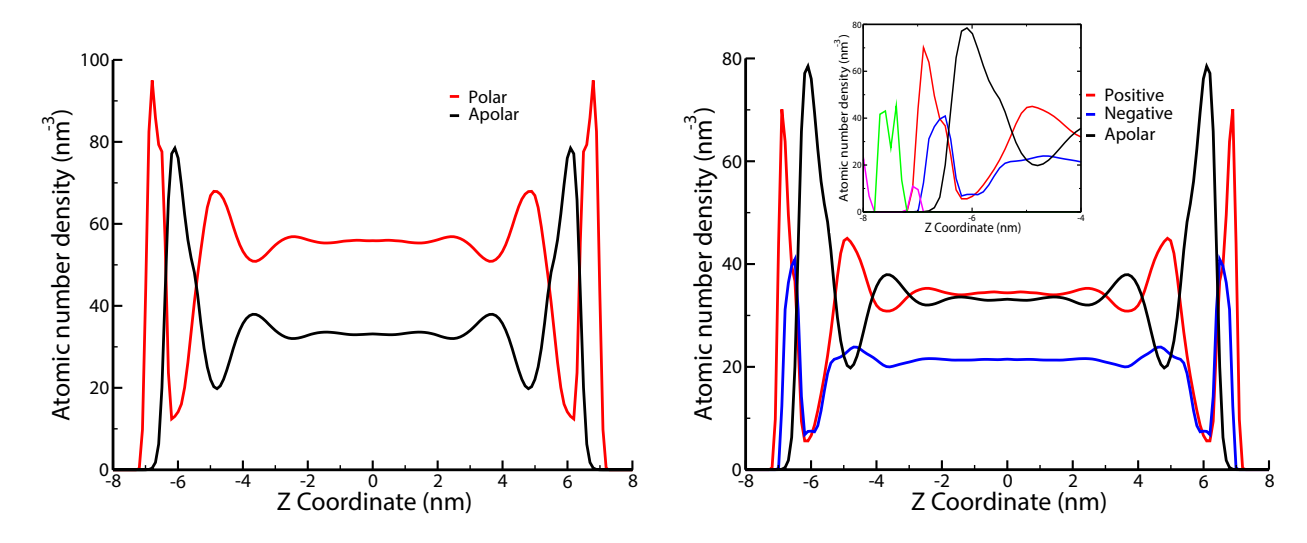


Figure 4: Polar–Apolar (left) and Positive–Negative–Apolar (right) symmetrized density profiles along the surface normal Z direction. Inset zooms into the interface to show also the atomic densities of K⁺ ions (magenta) and basal oxygen atoms (green) of (001) mica.

Next we focus on the effect of ionic size on their relative concentration along the z-axis and

away from the interface. In reference 32 we found significant enrichment of larger size ions at the vacuum interface. The more apolar ions formed a blocking layer effectively confining the smaller more polar ions to the interior of the interface and concealing them from vacuum. Density profiles in Figure 5 show that at the mica–IL interface both types of ions coexist. C[8]-mim⁺ and C[2]-mim⁺ heads have sharp density peaks at about the same z-coordinate. This behavior is clearly exemplified in Fig. 3 where both types of ion heads lay in grooves parallel to rows of K^+ with their tails pointing towards the liquid interior. Similarly, heads of C[2]-OSO $_3^-$ and C[8]-OSO $_3^-$ cap K^+ ions resulting in head density distributions with maxima at similar z values in Fig. 5.

Instead, ions in the second polar layer away from the interface, appear to be segregated by size. In this second polar layer, heads of the larger C[8]-mim⁺/C[8]-OSO₃⁻ ions appear predominantly first (-5.5 to -5 nm in Fig. 5), followed by those of the smaller C[2]-mim⁺/C[2]-OSO₃⁻ ions (-5 to -4.5 nm in Fig. 5). The reason for this "by–size" separation of ionic species is the formation of an apolar bilayer beneath the highly polar adlayer; the formation of this structure will become more apparent when we discuss the angular distribution of tails with respect to the z-axis, in the following subsection. Interestingly, in the case of confinement by a vacuum interface, the formation of an apolar bilayer and a separation of ions by size inside the liquid and away from the immediate interfacial apolar monolayer was also observed.³²

3.2 Orientational Order as a Function of distance from the Solid

A noticeably thick (\sim 2 nm) apolar density region separates the first and second polar regions discussed above, we see this not only from Figs. 4 and 5 but also from the system snapshot displayed in Fig. 2. For C[8]-mim⁺, in Fig. 6 we analyze the orientational order parameter defined as the average of the first Legendre polynomial, $P_1(\theta)$ where θ is the angle between a unit vector connecting the positions of the fourth-to-last and terminal tail carbon atoms. Results for C[8]-OSO₃⁻ are qualitatively similar and not shown. Along with $P_1(\theta)$ we also show in Fig. 6 polar and apolar carbon atom density profiles as well as the density profiles for

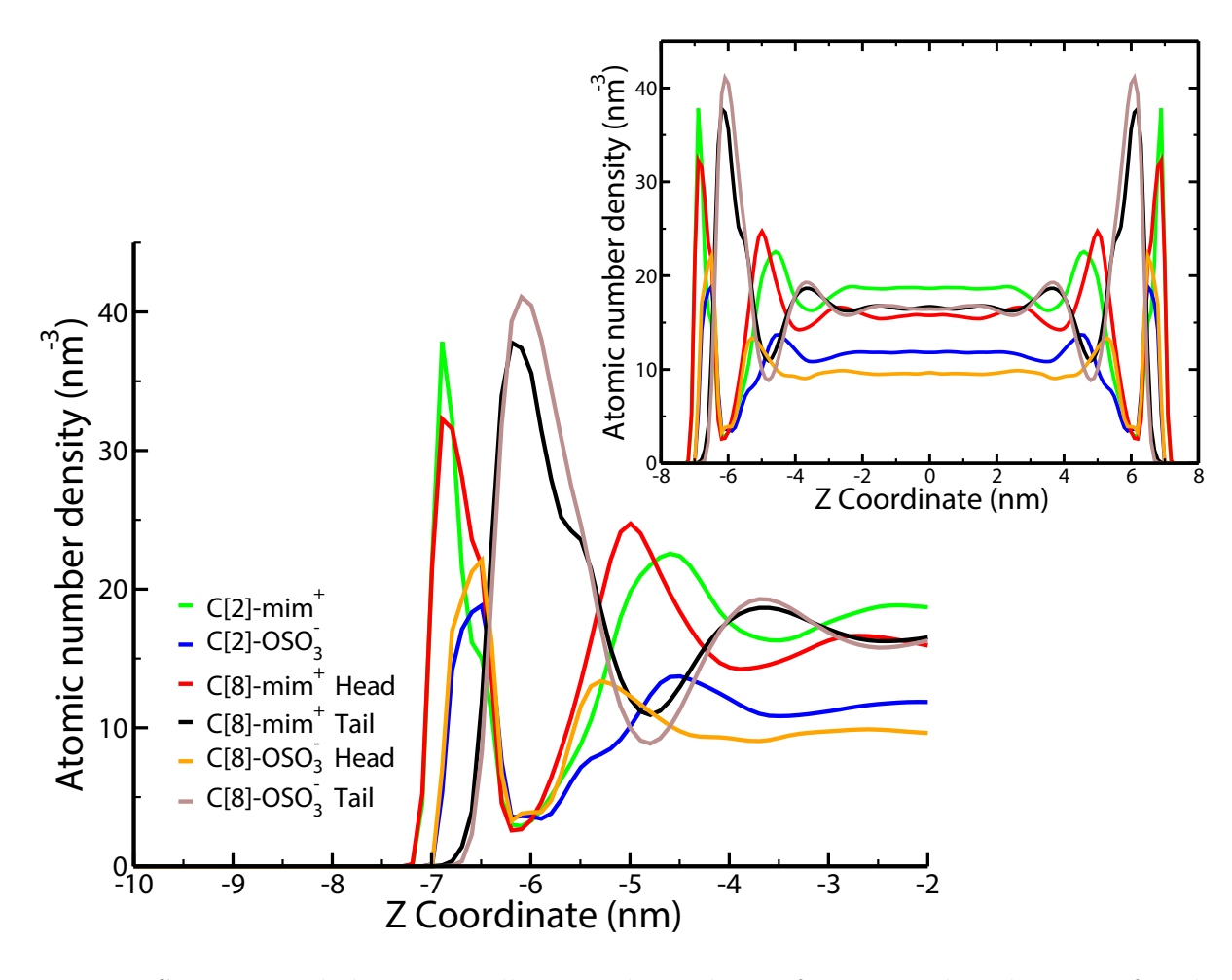


Figure 5: Symmetrized density oscillations along the surface normal Z direction for the positive, negative and apolar subcomponents of each ion. We show the symmetrized full density profile in the inset.

each individual carbon atom in the apolar tail of C[8]-mim⁺. Dashed vertical lines indicate the first two points where $P_1(\theta)$ crosses zero. In the immediate vicinity of mica, $P_1(\theta)$ is positive indicating that tails point away from the solid. Oscillatory angular orientation occurs away from the solid and fully decays within approximately 5 nm (the function is noisy at very low z values because there is almost no apolar tail density to average in that region).

We notice that the thick apolar region accommodates two distinct density peaks for every non-polar carbon atom (except for terminal C). The first set of carbon density peaks closest to the interface appear to the left of the first dashed vertical line, whereas the second set of peaks appear to the right. Differently said, for the most part, all tails attached to heads in the adlayer tend to point inwards towards the liquid phase whereas the second set of individual carbon density peaks correspond to tails pointing outwards towards the solid forming a bilayer. If we consider the behavior of $P_1(\theta)$ between the solid and the second vertical line away from the interface as a period, we can see that overall there are about 2.5 such periods beyond which both $P_1(\theta)$ and the density profiles become flat and bulk liquid-like structural behavior is recovered.

3.3 Lateral Layer Structure as a Function of Distance to the Mica Surface

So far, our description of the interface has been done by averaging over the x and y coordinates of liquid slabs to obtain distribution functions that are only z-dependent. In Fig. 7, we show instead zone–resolved tangential radial distribution functions (TRDFs) as defined in eqn. 1.⁶⁷

$$g_{ij}(r) = \frac{\sum_{i,j} \delta(r - r_{ij})}{2\pi r \rho_{zone} dr \Delta z}; \qquad r_{ij} = \sqrt{x_{ij}^2 + y_{ij}^2}$$

$$\tag{1}$$

where $\rho_{zone} = N_{zone}/(L_x L_y \Delta z)$. Each planar slab is chosen to be 0.5 nm in thickness and we focus our discussion on specific slabs that highlight three different zones in our simulation; the first slab corresponds to the adlayer or near–interfacial first polar peak (\sim -7.1 to -6.6

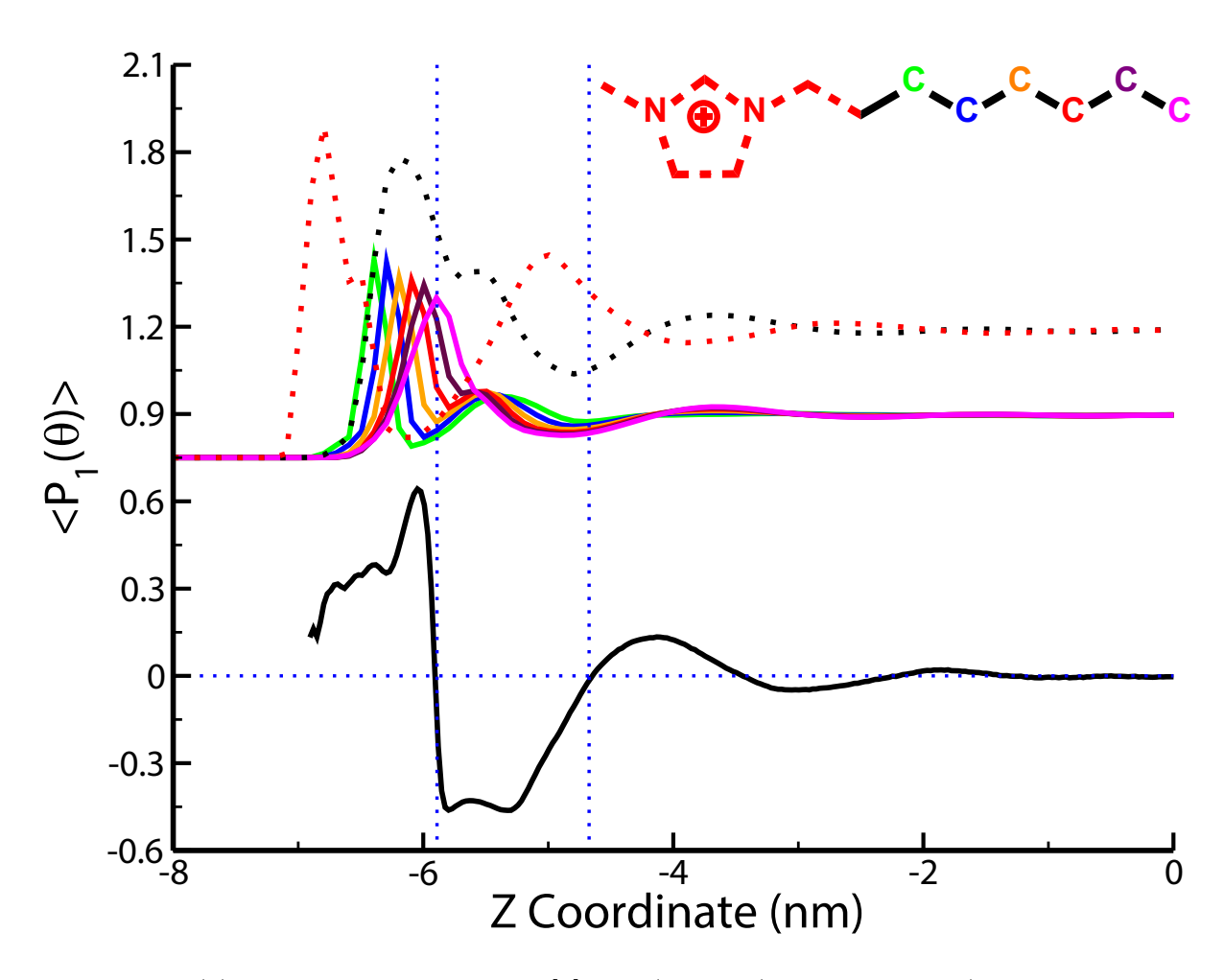


Figure 6: $P_1(\theta)$ order parameter for C[8]-mim⁺ tails (solid-black line). Positive values indicate that tails point away from the interface (towards the liquid) and negative values towards the interface. Vertically shifted and scaled are individual tail carbon atomic number density profiles as well as total polar and apolar carbon atom density profiles. Total polar and apolar carbon atom density profiles are represented with dotted red and black lines respectively and individual tail carbon atom density profiles are color coded the same way as the atoms in the inset.

nm in Fig. 4), the second slab highlights the second polar peak or sub–interfacial region (\sim -5.1 to -4.6 nm in Fig. 4) and the third slab is chosen from the bulk–like region (\sim -0.25 to 0.25 nm in Fig. 4).

Fig. 7, shows marked differences across TRDFs for the near—interfacial region when compared to the sub—interfacial and bulk regions. The near—interfacial IL mixture displays solid-like character—denoted by the repetitive and slowly decaying on-plane spatial correlations—but both the sub—interfacial and bulk—like regions have TRDFs that look liquid-like. Whereas the TRDFs in the sub—interfacial region and bulk—like regions look similar (but not identical), we know from Fig. 6 that the two regions must be structurally different in order for the sub—interfacial region to accommodate the non—random orientation of tails giving rise to the bilayer that is absent in the bulk. This begs the question of whether the small differences observed in the TRDFs in these two regions are linked to significant differences in dynamics and if the bulk—like region of a thin film has dynamical characteristics that can be considered the same as proper bulk.

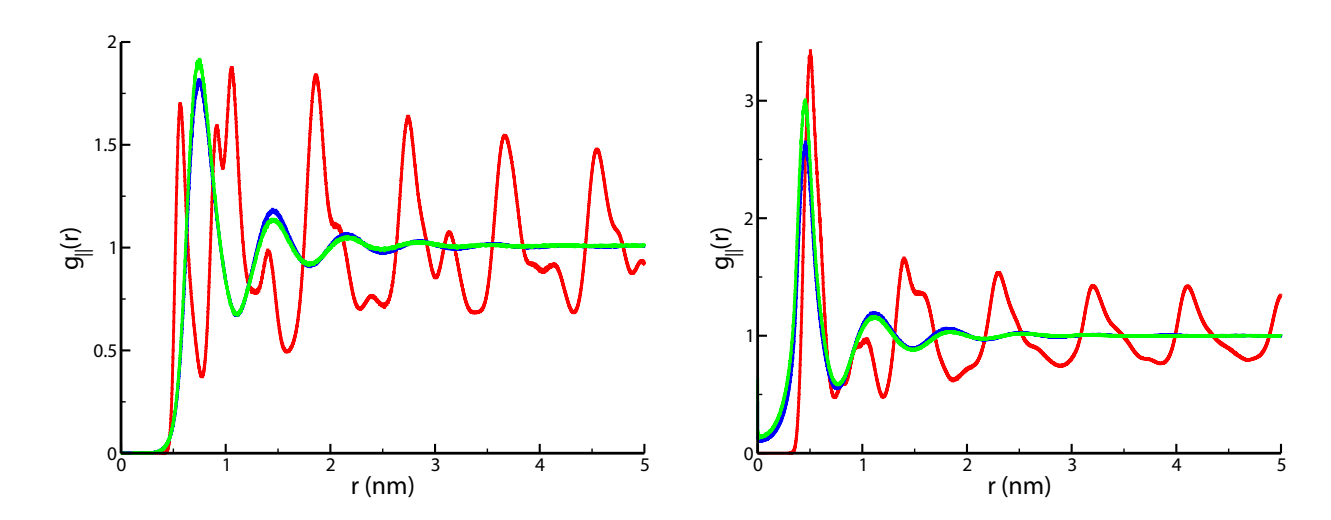


Figure 7: TRDFs for the S–S (left) and N–S (right) atomic correlations. Red, blue and green are for the adlayer, the sub–interfacial and bulk–like regions. The slab locations are based on the polar–apolar density profile as defined in the text of subsection 3.3.

3.4 Dynamics of Ions in Slabs at and Away From the Interface

For ions in different layers at and away from the interface, in this section we compare dynamical properties including the survival probability time correlation function and the lateral mean square displacement. Since for these properties we follow the position of ionic centers of mass, we chose our slabs based on maxima of their corresponding density profiles shown in Fig. S.1 of the SI.

The survival probability time correlation function defined in eqn. $2,^{68,69}$ computes the number of ions originally within a slab that remain in the slab at time t=m dt without ever leaving.

$$N(m dt) = \frac{1}{N_f - m} \sum_{j=1}^{N_{sys}} \sum_{n=1}^{N_f - m} p_j(n dt, m dt; dt)$$
 (2)

In our study, dt = 1 ps, n dt is the starting point in a collection of sliding windows of size m dt, N_f is the total number of initial frames and N_{sys} is the total number of ions of a given type in the system. If an ion j is inside a given slab at time n dt and remains so without ever leaving up to time (n dt+m dt), $p_j(n dt, m dt; dt)$ is 1, otherwise it is 0. N(0) gives the average number of ions of a given type in the slab. For ease of comparison, in Fig. 8 we plot the normalized survival probability time correlation function N(t)/N(0) corresponding to the fraction of ions remaining in the slab at time t.

From Fig. 8, we see that mica provides a very sticky interface, with ions from the IL mixture remaining there for very long times without being exchanged with others from adjacent layers. We notice that whereas distribution functions in Fig. 7 for the sub–interfacial and bulk–like regions may be quite similar, the mobility of ions may not be.

For slabs defined in Fig. 8, Fig. 9 shows the lateral mean square displacements as defined in eqn. 3, 69

$$MSD(t) = \frac{1}{N_{\text{Ion}'}(t)} \sum_{t_0}^{T_{run}-t} \sum_{j=1}^{N_{\text{Ion}}(t_0,t)} [r_j(t+t_0) - r_j(t_0)]^2$$
 (3)

where N_{Ion} is the number of ions of a given type in the slab at t_0 which remain there

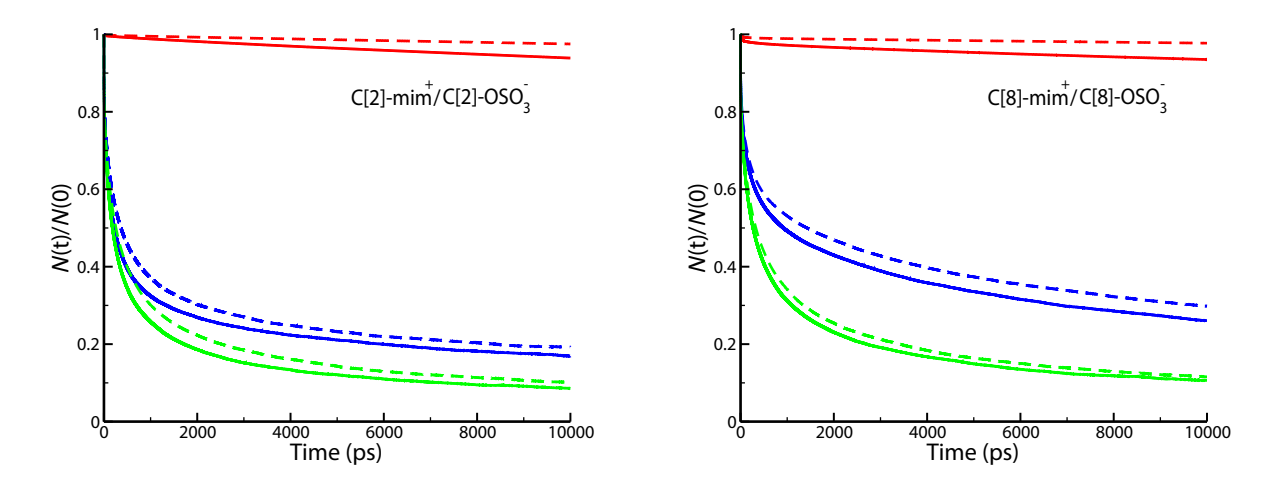


Figure 8: Normalized survival probability time correlation function in the near–intefacial (red), sub–interfacial (blue), and bulk–like (green) regions. Solid lines represent the cations and dashed lines represent the anions. Slab positions are chosen based on Fig. S.1 in the SI. For C[8]-mim⁺ near–interfacial region (-6.7 to -6.2 nm), sub–interfacial region (-5.5 to -5.0 nm); for C[8]-OSO $_3^-$ near–interfacial region (-6.7 to -6.2 nm), sub–interfacial region (-5.7 to -5.2 nm); for C[2]-mim⁺ near–interfacial region (-7.0 to -6.5 nm), sub–interfacial region (-4.8 to -4.3 nm); for C[2]-OSO $_3^-$ near–interfacial region (-6.9 to -6.4 nm), sub–interfacial region (-4.9 to -4.4 nm). In all cases the bulk–like region is taken to be between (-0.25 to 0.25 nm).

uninterruptedly until $t_0 + t$ and $N_{\text{Ion'}}(t)$ is defined in eqn 4.⁶⁹

$$N_{\text{Ion'}}(t) = \sum_{t_0}^{T_{run} - t} N_{\text{Ion}}(t_0, t)$$
(4)

The mean square displacements paint a picture similar to that of the survival probability function, where ions close to mica not only stay there but also do not significantly laterally diffuse. Notice that lateral diffusion in the sub–interfacial region is already very similar to that in the bulk–like region in the middle of the film; this is in contrast to what we see in the survival probability correlation function that is associated with the escape of ions in the surface normal z direction.

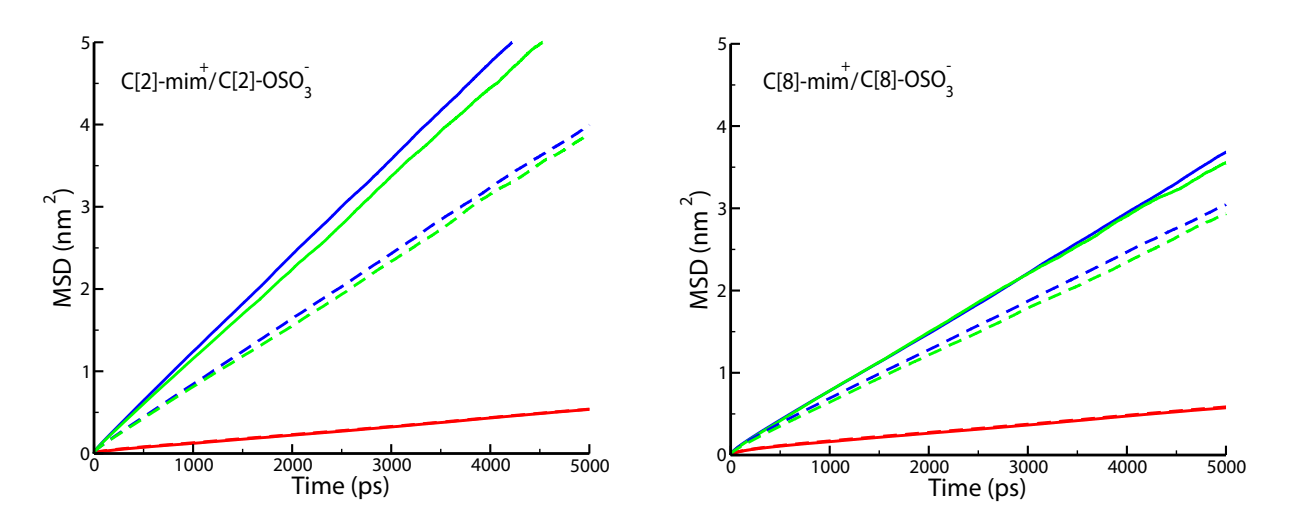


Figure 9: Lateral MSDs as computed from eqn. 3 are compared for the ions in the adlayer (red), sub-interfacial region (blue) and bulk-like region (green). Solid lines represent the cations and dashed lines represent the anions. Slab definitions are the same as used in Fig. 8.

3.5 How Different from Actual Bulk is the Bulk–Like Region of a Nanoscale IL Film?

In light of recent work hinting at the possibility that –even far from interfaces– structure and dynamical behavior could be different for ILs under confinement, we present results for slabs each of 0.5 nm width corresponding to the center of our thin films confined by vacuum, ³² mica and actual bulk. Because of our careful equilibration protocol, we know that the density in slabs associated with the bulk–like regions of our films match to within a small fraction of a percent that of our bulk simulations. This is important because liquids at different densities will have different distribution functions and transport properties.

For the three slabs, in Fig. 10 we show the tangential pair distribution function for cationic N coupled to anionic S. Other TRDFs associated with different correlations are provided in Figs. S.2 of the SI.

In Fig. 10, the three pair distribution functions are for practical purposes indistinguishable. Similar conclusions can be derived for other correlations presented in the SI. From this we learn that, for our systems, the bulk–like region just a few nanometers away from a very

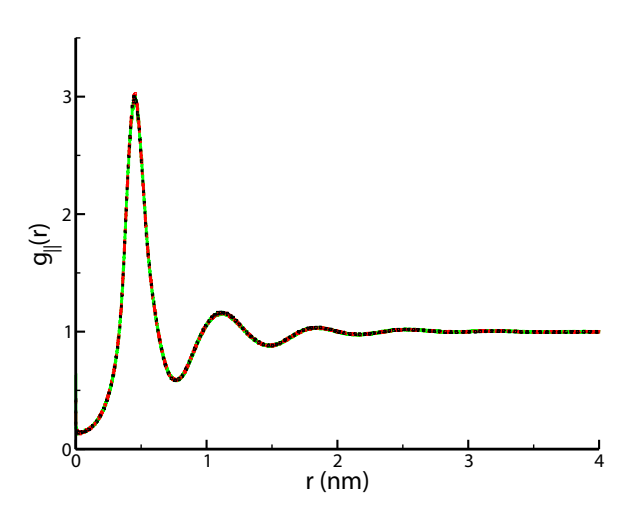


Figure 10: For the same IL mixture, TRDFs for the N–S correlation in slabs of (1) the unperturbed bulk phase (black), (2) the bulk–like region of a vacuum–surrounded film–³² (red) and (3) the bulk–like region of the mica–surrounded film– (green). Please see TRDFs for other mixture components in Figs. S.2 of the SI.

polar or a very apolar interface is structurally very similar to actual bulk.

Fig. 11 shows the normalized survival probability time correlation functions for centers of mass of C[2]-OSO₃⁻ (graphs for others ions are provided in Fig. S.3 of the SI). The functions are nearly identical indicating that movement of ions out of the bulk–like slabs occur on the same time–scale for both films and as in actual bulk. Fig. 11 shows that roughly 80% of ions leave the slab in about 2 ns.

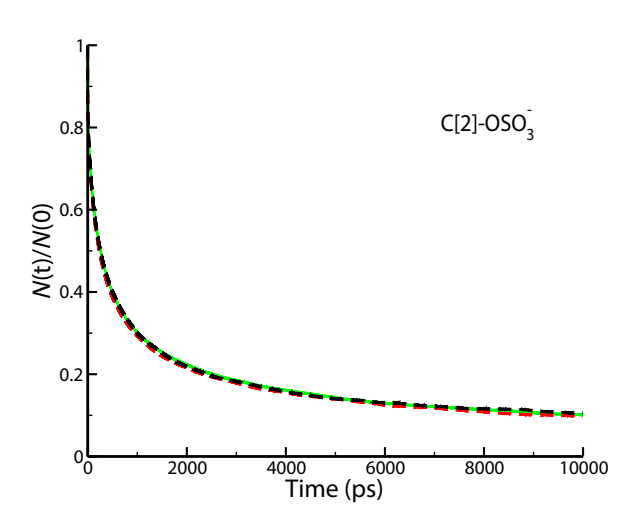


Figure 11: Comparison of the normalized survival probability time correlation functions for identical size slabs in the bulk–like region of mica–confined IL, vacuum–confined IL³² and actual bulk. Unperturbed bulk phase, bulk–like regions of vacuum– and mica–IL systems are color coded in black, red and green respectively. See also Fig. S.3 in the SI.

4 Conclusions

For a film consisting of 50% C[8]-mim⁺/C[8]-OSO₃⁻ and C[2]-mim⁺/C[2]-OSO₃⁻ at the mica interface, we find that the immediate adlayer is highly polar and that an apolar bilayer forms contiguous to it. The polar layer adjacent to the interface results from cationic and anionic charge group densities that are slightly displaced with respect to each other along the surface normal direction. Both types of ions (with short and long tails) significantly contribute to the adlayer; this is in contrast to a vacuum surrounded film for which the larger ions are the major contributors of density at the immediate interface.

For the film confined by mica, we find that interface—induced density oscillations fade away within a 5 nm decay correlation length giving rise to bulk—like liquid behavior. The structure of the liquid mixture at the adlayer is reminiscent of a solid, pair distributions in the sub–interfacial region are much more liquid—like. Yet, in this region, surface—induced order still persists as can be appreciated from tail orientational oscillations.

When comparing the bulk-like regions in the middle of our vacuum- and mica-surrounded

films against actual bulk simulations at the same density and temperature, we find them to be structurally and dynamically nearly indistinguishable. We find that as a function of distance to the interface, properties that probe structure and dynamics parallel to it appear to converge more quickly to bulk-like behavior. For example, whereas the density profiles, the angular order parameters and the survival probability time correlation functions are significantly different at the sub-interfacial layer when compared to the bulk, the lateral mean square displacement curves and the tangential radial distribution functions are more similar to those in the bulk. It is therefore possible that one may need to define a set of property-specific interfacial decorrelation length scales. However, it would appear that all properties converge to bulk behavior when the properly averaged z-dependent density profiles becomes flat, or in other words on the length scale of interfacial structural decorrelation.

5 Acknowledgments

This work was supported by NSF Grant No. 1664832 awarded to C.J.M.

6 Supporting Information

For our mixture of ILs, center of mass of the ions z-dependent density profiles when confined by mica, comparison of TRDFs and survival probability time correlation functions for mica—confined, vacuum—confined and unperturbed bulk slabs are provided in the Supporting Information free of charge on the ACS Publications website at DOI:XXX

References

(1) Araque, J. C.; Hettige, J. J.; Margulis, C. J. Modern Room Temperature Ionic Liquids, a Simple Guide to Understanding Their Structure and How It May Relate to Dynamics. J. Phys. Chem. B 2015, 119, 12727–12740.

- (2) Hayes, R.; Warr, G. G.; Atkin, R. Structure and Nanostructure in Ionic Liquids. *Chem. Rev.* **2015**, *115*, 6357–6426.
- (3) Greaves, T. L.; Drummond, C. J. Protic Ionic Liquids: Evolving Structure–Property Relationships and Expanding Applications. *Chem. Rev.* **2015**, *115*, 11379–11448.
- (4) Plechkova, N. V.; Seddon, K. R. In Methods and Reagents for Green Chemistry; Tundo, P., Perosa, A., Zecchini, F., Eds.; John Wiley & Sons, Inc.: New Jersey, 2007; Chapter 5, pp 103–130.
- (5) Feldmann, C.; Ruck, M. Ionic Liquids Designer Solvents for the Synthesis of New Compounds and Functional Materials. J. Inorg. Gen. Chem. 2017, 643, 2–2.
- (6) Macchieraldo, R.; Esser, L.; Elfgen, R.; Voepel, P.; Zahn, S.; Smarsly, B. M.; Kirchner, B. Hydrophilic Ionic Liquid Mixtures of Weakly and Strongly Coordinating Anions with and without Water. ACS Omega 2018, 3, 8567–8582.
- (7) Canales, R. I.; Held, C.; Lubben, M. J.; Brennecke, J. F.; Sadowski, G. Predicting the Solubility of CO₂ in Toluene + Ionic Liquid Mixtures with PC-SAFT. *Ind. Eng. Chem. Res.* **2017**, *56*, 9885–9894.
- (8) Brooks, N. J.; Castiglione, F.; Doherty, C. M.; Dolan, A.; Hill, A. J.; Hunt, P. A.; Matthews, R. P.; Mauri, M.; Mele, A.; Simonutti, R. et al. Linking the Structures, Free Volumes, and Properties of Ionic Liquid Mixtures. *Chem. Sci.* 2017, 8, 6359–6374.
- (9) Minnick, D. L.; Flores, R. A.; DeStefano, M. R.; Scurto, A. M. Cellulose Solubility in Ionic Liquid Mixtures: Temperature, Cosolvent, and Antisolvent Effects. J. Phys. Chem. B 2016, 120, 7906–7919.
- (10) Lall-Ramnarine, S. I.; Suarez, S. N.; Fernandez, E. D.; Rodriguez, C.; Wei, S.; Gobet, M.; Jayakody, J. R. P.; Dhiman, S. B.; Wishart, J. F. Exploring the Use of

- Ionic Liquid Mixtures to Enhance the Performance of Dicationic Ionic Liquids. *J. Electrochem. Soc.* **2017**, *164*, H5150–H5159.
- (11) Niedermeyer, H.; Hallett, J. P.; Villar-Garcia, I. J.; Hunt, P. A.; Welton, T. Mixtures of Ionic Liquids. *Chem. Soc. Rev.* **2012**, *41*, 7780–7802.
- (12) Fillion, J. J.; Brennecke, J. F. Viscosity of Ionic Liquid–Ionic Liquid Mixtures. *J. Chem. Eng. Data* **2017**, *62*, 1884–1901.
- (13) Cabry, C. P.; D'Andrea, L.; Shimizu, K.; Grillo, I.; Li, P.; Rogers, S.; Bruce, D. W.; Lopes, J. N. C.; Slattery, J. M. Exploring the Bulk-phase Structure of Ionic Liquid Mixtures using Small-angle Neutron Scattering. Faraday Discuss. 2018, 206, 265–289.
- (14) Ruiz, V.; Huynh, T.; Sivakkumar, S. R.; Pandolfo, A. G. Ionic Liquid–Solvent Mixtures as Supercapacitor Electrolytes for Extreme Temperature Operation. RSC Adv. 2012, 2, 5591–5598.
- (15) Dagousset, L.; Nguyen, G. T. M.; Vidal, F.; Galindo, C.; Aubert, P.-H. Ionic liquids and γ-butyrolactone Mixtures as Electrolytes for Supercapacitors Operating over Extended Temperature Ranges. RSC Adv. 2015, 5, 13095–13101.
- (16) Tariq, M.; Shimizu, K.; Esperança, J. M. S. S.; Lopes, J. N. C.; Rebelo, L. P. N. Viscosity Minima in Binary Mixtures of Ionic Liquids + Molecular Solvents. *Phys. Chem. Chem. Phys.* 2015, 17, 13480–13494.
- (17) Elbourne, A.; Votchovsky, K.; Warr, G. G.; Atkin, R. Ion Structure Controls Ionic Liquid Near-Surface and Interfacial Nanostructure. *Chem. Sci.* **2015**, *6*, 527–536.
- (18) Griffin, L. R.; Browning, K. L.; Clarke, S. M.; Smith, A. M.; Perkin, S.; Skoda, M. W. A.; Norman, S. E. Direct Measurements of Ionic Liquid Layering at a Single Mica-Liquid Interface and in Nano-films between Two Mica-Liquid Interfaces. *Phys. Chem. Chem. Phys.* 2017, 19, 297–304.

- (19) de Freitas, A. A.; Shimizu, K.; Smith, A. M.; Perkin, S.; Lopes, J. N. C. Structure and Dynamics of Mica-confined Films of [C₁₀C₁Pyrr][NTf₂] Ionic Liquid. *J. Chem. Phys.* **2018**, *148*, 193808.
- (20) Dragoni, D.; Manini, N.; Ballone, P. Interfacial Layering of a Room-Temperature Ionic Liquid Thin Film on Mica: A Computational Investigation. *ChemPhysChem* **2012**, *13*, 1772–1780.
- (21) Zhang, F.; Fang, C.; Qiao, R. Effects of Water on Mica–Ionic Liquid Interfaces. J. Phys. Chem. C 2018, 122, 9035–9045.
- (22) Zhang, H.; Zhu, M.; Zhao, W.; Li, S.; Feng, G. Molecular Dynamics Study of Room Temperature Ionic Liquids with Water at Mica Surface. *Green Energy & Environment* **2018**, *3*, 120–128.
- (23) Payal, R. S.; Balasubramanian, S. Orientational Ordering of Ionic Liquids near a Charged Mica Surface. *ChemPhysChem* **2012**, *13*, 1764–1771.
- (24) Payal, R. S.; Balasubramanian, S. Effect of Cation Symmetry on the Organization of Ionic Liquids near a Charged Mica Surface. J. Phys.: Condens. Matter 2014, 26, 284101.
- (25) Yokota, Y.; Miyamoto, H.; Imanishi, A.; Inagaki, K.; Morikawa, Y.; ichi Fukui, K. Structural and Dynamic Properties of 1-butyl-3-methylimidazolium bis(trifluoromethanesulfonyl)imide/Mica and Graphite Interfaces Revealed by Molecular Dynamics Simulation. *Phys. Chem. Chem. Phys.* **2018**, *20*, 6668–6676.
- (26) Jurado, L. A.; Kim, H.; Arcifa, A.; Rossi, A.; Leal, C.; Spencer, N. D.; Espinosa-Marzal, R. M. Irreversible Structural Change of a Dry Ionic Liquid under Nanoconfinement. Phys. Chem. Chem. Phys. 2015, 17, 13613–13624.

- (27) Parr, D.; Chrestenson, J.; Malik, K.; Molter, M.; Zibart, C.; Egan, B.; Haverhals, L. M. Structure and Dynamics at Ionic Liquid/Electrode Interfaces. *ECS Trans.* **2015**, *66*, 35–42.
- (28) Anaredy, R. S.; Shaw, S. K. Long-Range Ordering of Ionic Liquid Fluid Films. *Langmuir* **2016**, *32*, 5147–5154.
- (29) Shin, J. Y.; Yamada, S. A.; Fayer, M. D. Dynamics of a Room Temperature Ionic Liquid in Supported Ionic Liquid Membranes vs the Bulk Liquid: 2D IR and Polarized IR Pump-Probe Experiments. J. Am. Chem. Soc. 2016, 139, 311–323.
- (30) Shin, J. Y.; Yamada, S. A.; Fayer, M. D. Carbon Dioxide in a Supported Ionic Liquid Membrane: Structural and Rotational Dynamics Measured with 2D IR and Pump-Probe Experiments. J. Am. Chem. Soc. 2017, 139, 11222–11232.
- (31) Nishida, J.; Breen, J. P.; Wu, B.; Fayer, M. D. Extraordinary Slowing of Structural Dynamics in Thin Films of a Room Temperature Ionic Liquid. ACS Cent. Sci. 2018, 4, 1065–1073.
- (32) Wu, F.; Karunaratne, W. V.; Margulis, C. J. Ionic Liquid Mixture at the Vacuum Interface and the Peaks and Antipeaks Analysis of X-ray Reflectivity. *J. Phys. Chem.* C 2019, 123, 4914–4925.
- (33) Elbourne, A.; Sweeney, J.; Webber, G. B.; Wanless, E. J.; Warr, G. G.; Rutland, M. W.; Atkin, R. Adsorbed and Near-surface Structure of Ionic Liquids Determines Nanoscale Friction. *Chem. Commun. (Cambridge, U. K.)* **2013**, *49*, 6797–6799.
- (34) Segura, J. J.; Elbourne, A.; Wanless, E. J.; Warr, G. G.; Votchovsky, K.; Atkin, R. Adsorbed and Near Surface Structure of Ionic Liquids at a Solid Interface. *Phys. Chem. Chem. Phys.* 2013, 15, 3320–3328.

- (35) Nagy, K. L.; Cygan, R. T.; Hanchar, J. M.; Sturchio, N. C. Gibbsite Growth Kinetics on Gibbsite, Kaolinite, and Muscovite Substrates: Atomic Force Microscopy Evidence for Epitaxy and an Assessment of Reactive Surface Area. Geochim. Cosmochim. Acta 1999, 63, 2337–2351.
- (36) Christenson, H. K.; Thomson, N. H. The Nature of the Air-cleaved Mica Surface. Surf. Sci. Rep. 2016, 71, 367–390.
- (37) Bampoulis, P.; Sotthewes, K.; Siekman, M. H.; Zandvliet, H. J. W.; Poelsema, B. Graphene Visualizes the Ion Distribution on Air-Cleaved Mica. Sci. Rep. 2017, 7, 43451.
- (38) Gong, X.; Kozbial, A.; Li, L. What Causes Extended Layering of Ionic Liquids on the Mica Surface? *Chem. Sci.* **2015**, *6*, 3478–3482.
- (39) Cheng, H.-W.; Stock, P.; Moeremans, B.; Baimpos, T.; Banquy, X.; Renner, F. U.; Valtiner, M. Characterizing the Influence of Water on Charging and Layering at Electrified Ionic-Liquid/Solid Interfaces. *Adv. Mater. Interfaces* **2015**, 2, 1500159.
- (40) Cheng, H.-W.; Dienemann, J.-N.; Stock, P.; Merola, C.; Chen, Y.-J.; Valtiner, M. The Effect of Water and Confinement on Self-Assembly of Imidazolium Based Ionic Liquids at Mica Interfaces. *Sci. Rep.* **2016**, *6*, 30058.
- (41) Kobayashi, K.; Liang, Y.; ichi Amano, K.; Murata, S.; Matsuoka, T.; Takahashi, S.; Nishi, N.; Sakka, T. Molecular Dynamics Simulation of Atomic Force Microscopy at the Water-Muscovite Interface: Hydration Layer Structure and Force Analysis. *Langmuir* 2016, 32, 3608-3616.
- (42) Higginbotham, I. G.; Williams, R. H.; McEvoy, A. J. Metal/Non-Metal Interfaces: Adhesion of Gold on Mica. J. Phys. D: Appl. Phys. 1975, 8, 1033–1043.

- (43) Odelius, M.; Bernasconi, M.; Parrinello, M. Two Dimensional Ice Adsorbed on Mica Surface. *Phys. Rev. Lett.* **1997**, *78*, 2855–2858.
- (44) Cheng, L.; Fenter, P.; Nagy, K. L.; Schlegel, M. L.; Sturchio, N. C. Molecular-Scale Density Oscillations in Water Adjacent to a Mica Surface. *Phys. Rev. Lett.* 2001, 87, 156103.
- (45) Richardson, S. M.; James W. Richardson, J. Crystal Structure of a Pink Muscovite from Archer's Post, Kenya: Implications for Reverse Pleochroism in Dioctahedral Micas. Am. Mineral. 1982, 67, 69–75.
- (46) Sakuma, H.; Kawamura, K. Structure and Dynamics of Water on Li⁺-, Na⁺-, K⁺-, Cs⁺-, H₃O⁺-Exchanged Muscovite Surfaces: A Molecular Dynamics Study. *Geochim. Cosmochim. Acta* **2011**, *75*, 63–81.
- (47) Sakuma, H.; Kawamura, K. Structure and Dynamics of Water on Muscovite Mica Surfaces. *Geochim. Cosmochim. Acta* **2009**, *73*, 4100–4110.
- (48) Wang, J.; Kalinichev, A. G.; Kirkpatrick, R. J.; Cygan, R. T. Structure, Energetics, and Dynamics of Water Adsorbed on the Muscovite (001) Surface: A Molecular Dynamics Simulation. J. Phys. Chem. B 2005, 109, 15893–15905.
- (49) Cygan, R. T.; Liang, J.-J.; Kalinichev, A. G. Molecular Models of Hydroxide, Oxyhydroxide, and Clay Phases and the Development of a General Force Field. J. Phys. Chem. B 2004, 108, 1255–1266.
- (50) Lopes, J. N. C.; Deschamps, J.; Padua, A. A. H. Modeling Ionic Liquids Using a Systematic All-Atom Force Field. *J. Phys. Chem. B* **2004**, *108*, 2038–2047.
- (51) Lopes, J. N. C.; Padua, A. A. H.; Shimizu, K. Molecular Force Field for Ionic Liquids IV: Trialkylimidazolium and Alkoxycarbonyl-Imidazolium Cations; Alkylsulfonate and Alkylsulfate Anions. J. Phys. Chem. B 2008, 112, 5039–5046.

- (52) Jorgensen, W. L.; Maxwell, D. S.; Tirado-Rives, J. Development and Testing of the OPLS All-Atom Force Field on Conformational Energetics and Properties of Organic Liquids. J. Am. Chem. Soc. 1996, 118, 11225–11236.
- (53) Mcdonald, N. A.; Jorgensen, W. L. Development of an All-Atom Force Field for Heterocycles. Properties of Liquid Pyrrole, Furan, Diazoles, and Oxazoles. J. Phys. Chem. B 1998, 102, 8049–8059.
- (54) Price, M. L. P.; Ostrovsky, D.; Jorgensen, W. L. Gas-Phase and Liquid-State Properties of Esters, Nitriles, and Nitro Compounds with the OPLS-AA Force Field. J. Comput. Chem. 2001, 22, 1340–1352.
- (55) Brkljača, Z.; Klimczak, M.; Miličević, Z.; Weisser, M.; Taccardi, N.; Wasserscheid, P.; Smith, D. M.; Magerl, A.; Smith, A.-S. Complementary Molecular Dynamics and X-ray Reflectivity Study of an Imidazolium-Based Ionic Liquid at a Neutral Sapphire Interface. J. Phys. Chem. Lett 2015, 6, 549–555.
- (56) Hess, B.; Kutzner, C.; van der Spoel, D.; Lindahl, E. GROMACS 4: Algorithms for Highly Efficient, Load-Balanced, and Scalable Molecular Simulation. J. Chem. Theory Comput. 2008, 4, 435–447.
- (57) Van Der Spoel, D.; Lindahl, E.; Hess, B.; Groenhof, G.; Mark, A. E.; Berendsen, H. J. C. GROMACS: Fast, Flexible, and Free. J. Comput. Chem. 2005, 26, 1701–1718.
- (58) Abraham, M. J.; Murtola, T.; Schulz, R.; Páll, S.; Smith, J. C.; Hess, B.; Lindahl, E. GROMACS: High Performance Molecular Simulations through Multi-level Parallelism from Laptops to Supercomputers. *SoftwareX* **2015**, *1-2*, 19–25.
- (59) Nosé, S. A Unified Formulation of the Constant Temperature Molecular Dynamics Methods. J. Chem. Phys. 1984, 81, 511–519.

- (60) Nosé, S. A Molecular Dynamics Method for Simulations in the Canonical Ensemble.

 Mol. Phys 1984, 52, 255–268.
- (61) Hockney, R.; Goel, S.; Eastwood, J. Quiet High-Resolution Computer Models of a Plasma. J. Comput. Phys. 1974, 14, 148–158.
- (62) Parrinello, M.; Rahman, A. Polymorphic Transitions in Single Crystals: A New Molecular Dynamics Method. J. Appl. Phys. 1981, 52, 7182–7190.
- (63) Darden, T.; York, D.; Pedersen, L. Particle Mesh Ewald: An N log(N) Method for Ewald Sums in Large Systems. J. Chem. Phys. 1993, 98, 10089–10092.
- (64) Essmann, U.; Perera, L.; Berkowitz, M. L.; Darden, T.; Lee, H.; Pedersen, L. G. A Smooth Particle Mesh Ewald Method. J. Chem. Phys. 1995, 103, 8577–8593.
- (65) Yeh, I.-C.; Berkowitz, M. L. Ewald Summation for Systems with Slab Geometry. *J. Chem. Phys.* **1999**, *111*, 3155–3162.
- (66) Yeh, I.-C.; Wallqvist, A. On the Proper Calculation of Electrostatic Interactions in Solid-Supported Bilayer Systems. *J. Chem. Phys.* **2011**, *134*, 055109.
- (67) Paredes, X.; Fernández, J.; Pádua, A. A. H.; Malfreyt, P.; Malberg, F.; Kirchner, B.; Pensado, A. S. Bulk and Liquid-Vapor Interface of Pyrrolidinium-Based Ionic Liquids: A Molecular Simulation Study. J. Phys. Chem. B 2014, 118, 731-742.
- (68) Impey, R. W.; Madden, P. A.; McDonald, I. R. Hydration and Mobility of Ions in Solution. J. Phys. Chem. 1983, 87, 5071–5083.
- (69) Chung, Y.-H.; Xia, J.; Margulis, C. J. Diffusion and Residence Time of Hydrogen Peroxide and Water in Crowded Protein Environments. J. Phys. Chem. B 2007, 111, 13336–13344.

TOC Graphic

